

# Monte Carlo model of acoustic response from a bubble cloud

Alexei Kouzoubov

Maritime Division, Defence Science and Technology Group, Edinburgh, Australia

## ABSTRACT

In various sonar applications it is important to model the acoustic response of a bubble cloud to a sonar pulse of different types. In a typical approximate approach, a bubble cloud is modelled as a set of point scatterers. The purpose of this research is to analyse the accuracy and limitation of such a representation. For this, a high-fidelity Monte Carlo model of scattering of an acoustic pulse from a bubble cloud is developed. In this model a bubble cloud is represented by a set of individual bubbles randomly selected from a known bubble size and spatial distribution. The acoustic signals scattered from individual bubbles are coherently summed into a collective response from the bubble cloud. The building block of the model is the forced oscillations of an individual bubble in an acoustic field. In this research we use the state-of-the-art equation of bubble oscillation. We then consider the acoustic response of a bubble cloud to an acoustic pulse in single scattering approximation and compare it with the analytically calculated backscattering cross section per unit volume. A comparison of the results of the high-fidelity model with the representation of the bubble cloud by a set of discrete scatterers is conducted.

## 1 INTRODUCTION

Modern simulations of sonar performance in military applications require higher fidelity models of sonar echoes from underwater objects. Various bubbly wakes play important part in these simulations. Examples of such wakes are surface ship wakes, exhaust gas bubbles behind a torpedo, the bubble cloud created by an underwater explosion. All of them can be described as bubble clouds of certain shape with a certain size and spatial distribution of bubbles. All these parameters define how a pulse from an active sonar will be scattered by a bubble cloud. In the current approach to sonar simulation, bubbly wakes are modelled as a set of point scatterers. It is of interest, therefore, to analyse the accuracy and limitation of such a representation. For this, a high-fidelity model of scattering of an acoustic pulse from a bubble cloud should be developed. Here we consider a Monte Carlo type model. In this model a bubble cloud is represented by a set of individual bubbles randomly selected from a known bubble size and spatial distribution. The acoustic signals scattered from individual bubbles are summed coherently into a collective response from the bubble cloud. Acoustic interaction between bubbles is ignored. The main element of the model is the forced oscillations of an individual bubble in an acoustic field of incident acoustic pulse. In this article we will describe the equation of bubble oscillation and verification of its numerical implementation by comparison of a numerically calculated acoustic scattering cross section of an individual bubble with the analytical solution of a linearized equation of bubble oscillation. We then consider the acoustic response of a bubble cloud to different acoustic pulses in the single scattering approximation and compare it with the analytically calculated backscattering cross section per unit volume. A comparison of the results of the high-fidelity model with the representation of the bubble cloud by a set of discrete scatterers will be conducted.

## 2 MODEL DESCRIPTION

### 2.1 Forced oscillation of an individual bubble

We base our model on the following equation of the forced oscillation of an individual bubble originally derived in Keller and Miksis (1980). Here we write it in the form presented in (Zhang 2013, Zhang and Li 2015):

$$\left(1 - \frac{\dot{R}}{c_l}\right) R \ddot{R} + \frac{3}{2} \left(1 - \frac{\dot{R}}{3c_l}\right) \dot{R}^2 = \left(1 + \frac{\dot{R}}{c_l}\right) \frac{p_{ext}(R,t) - p_s(t)}{\rho_l} + \frac{R}{\rho_l c_l} \frac{d[p_{ext}(R,t) - p_s(t)]}{dt} \quad (1)$$

where

$$p_{ext}(R, t) = \left(P_0 + \frac{2\sigma}{R_0}\right) \left(\frac{R_0}{R}\right)^{3\kappa} - \frac{4(\mu_l + \mu_{th})}{R} \dot{R} - \frac{2\sigma}{R}, \quad (2)$$

Here,  $R$  is the instantaneous bubble radius, the overdot denotes the time derivative;  $c_l$  is the speed of sound in the liquid;  $\rho_l$  is the density of the liquid;  $t$  is the time;  $P_0$  is the ambient pressure;  $\sigma$  is the coefficient of surface tension;  $R_0$  is the equilibrium bubble radius;  $\kappa$  is the polytropic exponent;  $\mu_l$  is the viscosity of the liquid;  $\mu_{th}$  is

the additional effective “thermal” viscosity;  $p_s(t)$  is the pressure outside the bubble at bubble wall. For a continuous wave (CW) acoustic signal of frequency  $f_s$ ,  $p_s(t)$  can be expressed as

$$p_s(t) = P_0[1 + \varepsilon_s \cos(2\pi f_s t)]. \quad (3)$$

where  $\varepsilon_s$  is the non-dimensional amplitude of the external pressure oscillation.

According to (Prosperetti 1977) the effective thermal viscosity and the polytropic exponent can be expressed as

$$\mu_{th} = \frac{1}{4} \omega \rho_g R_0^2 \text{Im}\varphi, \quad (4)$$

$$\kappa = \frac{1}{3} (\omega^2 \rho_g R_0^2 / P_{in,eq}) \text{Re}\varphi, \quad (5)$$

where  $\omega = 2\pi f_s$  and  $P_{in,eq} = P_0 + \frac{2\sigma}{R_0}$ . The parameter  $\varphi$  is defined as (Prosperetti 1977)

$$\varphi = \frac{kf(\Gamma_2 - \Gamma_1) + \lambda_2 \Gamma_2 - \lambda_1 \Gamma_1}{kf(\lambda_2 \Gamma_1 - \lambda_1 \Gamma_2) - \lambda_1 \lambda_2 (\Gamma_2 - \Gamma_1)}, \quad (6)$$

where

$$\Gamma_{1,2} = i + G_1 \pm [(i - G_1)^2 + 4iG_1/\gamma]^{1/2}, \quad (7)$$

$$\lambda_i = \beta_i \coth \beta_i - 1, \quad i = 1, 2, \quad (8)$$

$$\beta_{1,2} = \left( \frac{1}{2} \gamma G_2 \{ i - G_1 \pm [(i - G_1)^2 + 4iG_1/\gamma]^{1/2} \} \right)^{1/2}, \quad (9)$$

$$f = 1 + (1 + i) \left( \frac{1}{2} G_3 \right)^{1/2}. \quad (10)$$

In the above equations the following dimensionless parameters are introduced:

$$G_1 = M_g D_g \omega / \gamma R_g T_\infty, \quad G_2 = \omega R_0^2 / D_g, \quad G_3 = \omega R_0^2 / D_l,$$

where  $M_g$  is the molecular weight of the gas contained in the bubble,  $D_g = k_g / \rho_g c_{v,g}$  is its thermal diffusivity,  $\gamma = c_{p,g} / c_{v,g}$  is the ratio of its specific heats,  $R_g$  is the universal gas constant,  $T_\infty$  is the liquid temperature,  $D_l = k_l / \rho_l c_{v,l}$  is the thermal diffusivity of the liquid, and  $k = k_l / k_g$  is the ratio between the liquid and gas thermal conductivities.

The radiation pressure at the distance  $r$  from the bubble centre can be given as (Yang and Church 2005):

$$P_{rad}(r, t) = \frac{\rho_l R}{r} (2\dot{R}^2 + R\ddot{R}). \quad (11)$$

The integral characteristic of the acoustic scattering from a bubble is the total acoustical scattering cross section defined as (Wildt 1946)

$$\sigma_s = 4\pi |B/A|^2. \quad (12)$$

Here,  $A$  is the amplitude of the incident wave,  $B$  is the amplitude of the divergent spherical scattered wave generated by bubble oscillations at the distance of 1 m from the bubble centre. So the amplitude of the radiated pressure can be written as

$$|P_{rad}| = \left| \frac{B}{r} \right|. \quad (13)$$

It is interesting to compare the acoustic scattering cross-section obtained from the non-linear solution of the equation (1) with the analytical solution obtained from a linear approximation of the equation (1) for the case of

small-amplitude bubble oscillations. The analytical solution used for this comparison is taken from (Zhang 2013). We reproduce it here for completeness:

$$\sigma_s = \frac{4\pi R_0^2}{\left| M \left\{ \left[ \frac{\omega_0^2}{\omega^2} - 1 \right] + \left[ \frac{4(\mu_l + \mu_{th})}{M\omega\rho_l R_0^2} + \frac{R_0}{\omega c_l} \omega_0^2 \right] i \right\} \right|^2}, \quad (14)$$

where

$$\omega_0^2 = \frac{3\kappa(P_0 + 2\sigma/R_0) - 2\sigma/R_0}{\rho_l R_0^2 M}, \quad (15)$$

$$M = 1 + \frac{R_0}{c_l} \frac{4(\mu_l + \mu_{th})}{\rho_l R_0^2}. \quad (16)$$

The effective thermal viscosity  $\mu_{th}$  and the polytropic exponent  $\kappa$  are given by the above equations (4)-(5), with the parameter  $\varphi$  given by the above equations (6)-(10) reproduced from (Prosperetti 1977), where approximate expressions for equations (6)-(10) were also provided. These expressions were recently reproduced in (Zhang and Li 2014). Another analytical solution for  $\sigma_s$  is reproduced in (Medwin and Clay 1998) from the work of Eller (1970), which in its turn is based on work by Devin (1959).

Comparison between non-linear and analytical solutions was conducted for an air bubble in water. The equilibrium bubble radius varied in the range  $10\mu m \leq R_0 \leq 1mm$  with a step of  $1\mu m$ . The acoustic frequency of external pressure wave is  $f_s = 10kHz$ . Two values of the pressure wave non-dimensional amplitude,  $\varepsilon_s$ , are used in the numerical solution of equation (1): 0.01 and 0.1. Continuous wave pulse of 100 cycles length was used in this simulation. The results are shown in Figure 1. One can see from the figure that the numerical solution at smaller amplitude is close to the analytical solution. The numerical solution at larger amplitude deviates from the analytical solution significantly near the main resonance and at an additional resonance at lower non-dimensional frequency.

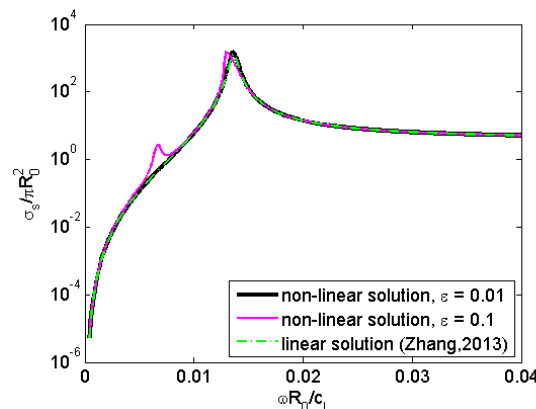


Figure 1. Normalized acoustic scattering cross-section. Comparison between non-linear and linear analytical solution.

It should be noted here that it takes several cycles for bubble oscillations to settle into the steady mode. To calculate the amplitude of radiated pressure the second half of the scattered pulse was used where oscillations were already settled into the steady mode. However, when we consider the combined scattered pulse from many bubbles, we will not be able to separate the steady mode response. It is, therefore, of interest to see how different the scattering cross-section calculated from steady oscillations is to that calculated from the whole pulse. The amplitude of the radiated pressure is calculated as the peak-to-peak value:

$$|P_{rad}| = \max(P_{rad}) - \min(P_{rad}). \quad (17)$$

One can see from Figure 2 that at some frequencies the scattering cross-section calculated from the whole pulse is higher than that calculated from the steady oscillations. This occurs in the areas adjacent to resonance but not at resonance itself.

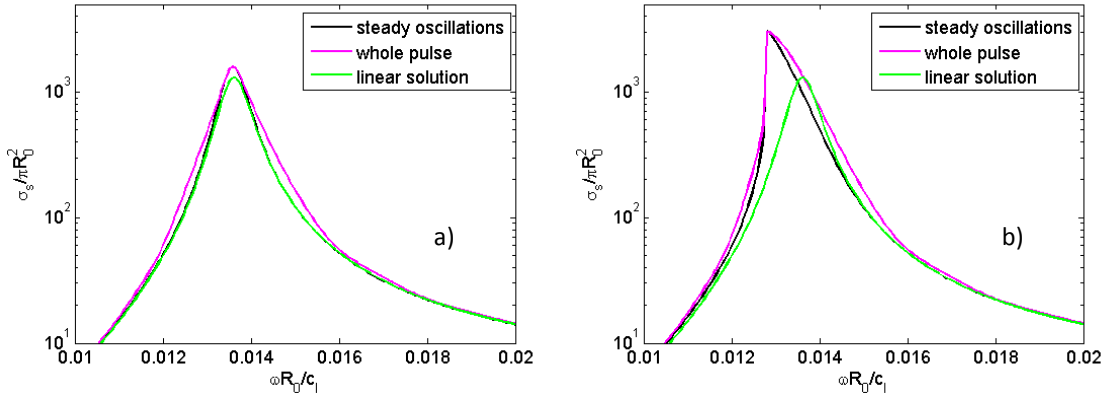


Figure 2. Scattering cross-section calculated from steady oscillations and whole pulse. a):  $\epsilon_s = 0.01$ ; b):  $\epsilon_s = 0.1$ .

In the case of pulses of finite length, it is more correct to use the pulse acoustic energy in the definition of the scattering cross-section. So, equation (12) should be written as:

$$\sigma_s = 4\pi E_s / E_i, \quad (18)$$

where  $E_i$  and  $E_s$  are the energy of the incident and scattered pulses, respectively:

$$E_i = \int p_i^2(t) dt, \quad (19)$$

$$E_s = \int p_s^2(t) dt, \quad (20)$$

where integration is performed over the pulse duration.

## 2.2 Scattering from an ensemble of non-interacting bubbles

Here we consider simulation of the acoustic response of an ensemble of bubbles to an incident acoustic pulse. Bubbles are assumed acoustically non-interacting with each other, in other words: multiple scattering is ignored. The resulting scattered pulse is a coherent summation of pulses scattered by individual bubbles contained in the insonified volume.

$$P_{bc} = \sum_{k=1}^{N_b} P_s(t; R_{0k}, R_{tb}^{(k)}, R_{rb}^{(k)}), \quad (21)$$

where  $N_b$  is the number of bubbles in the insonified volume,  $t$  is the time,  $R_{0k}$  is the equilibrium radius of the  $k$ th bubble,  $R_{tb}^{(k)}$  and  $R_{rb}^{(k)}$  is the distance from  $k$ th bubble to the transmitter and receiver, respectively.

The insonified volume is defined by the geometry of the sonar beam and the pulse length. In the simulation considered in this section we use a beam geometry based on that of the Imagenex profiling sonar (Imagenex 2015), which is a pencil beam with a small beam angle of about 2 degrees. The angle slightly depends on the sonar frequency, and here we assume the frequency of  $f_s = 450 \text{ kHz}$  and the beam angle  $\gamma = 2^\circ$ . The pulse length is  $\tau = 100 \mu\text{s}$ . The volume insonified by a sonar pulse is illustrated in Figure 3 with a few randomly positioned bubbles. The length of the volume is  $0.5c_1\tau$ . The volume of the insonified beam element is

$$V = \frac{1}{3}\pi \left\{ \left( r + \frac{1}{4}c_1\tau \right)^3 - \left( r - \frac{1}{4}c_1\tau \right)^3 \right\} \tan^2 \left( \frac{\gamma}{2} \right), \quad (22)$$

where  $r$  is the distance from the transmitter to the centre of the beam element.

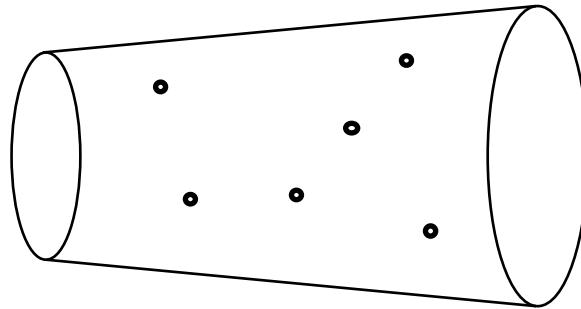


Figure 3. Insonified volume illustration.

Bubble sizes and their position in the insonified volume are selected randomly. The bubble sizes were generated from the power bubble size distribution:  $ndR = AR^{-m}dR$ , where the coefficient  $A$  is calculated from the given gas volume fraction,  $v_f$ , and the volume of the insonified beam element,  $V$ :

$$A = \frac{3(4-m)v_fV}{4\pi(R_{\max}^{4-m} - R_{\min}^{4-m})}, \quad (23)$$

where  $R_{\min}$  and  $R_{\max}$  are the minimum and maximum bubble radius in the bubble size distribution.

The total number of bubbles of all sizes in the insonified volume is

$$N_{bs} = \int_{R_{\min}}^{R_{\max}} ndR = \frac{A}{1-m} (R_{\max}^{1-m} - R_{\min}^{1-m}). \quad (24)$$

Thus, assuming the above bubble size distribution, the size of a bubble is calculated as

$$R = [R_{\min}^{1-m} + u(R_{\max}^{1-m} - R_{\min}^{1-m})]^{\frac{1}{1-m}}, \quad (25)$$

where  $u$  is a random, uniformly distributed number,  $0 \leq u \leq 1$ . The bubble size distribution for the random realisation is then obtained by binning the obtained bubble sizes into the specified size intervals  $[R_k, R_k + \Delta R]$ . In this simulation we used the following values:  $R_{\min} = 4 \mu m$ ,  $R_{\max} = 40 \mu m$ ,  $\Delta R = 0.1 \mu m$ , and  $v_f = 10^{-6}$ . This results in 1492514 bubbles in a single realisation of the bubble population in the insonified beam element. Bubble size distribution for a single realisation and that averaged over 500 realisations are shown in Figure 4.

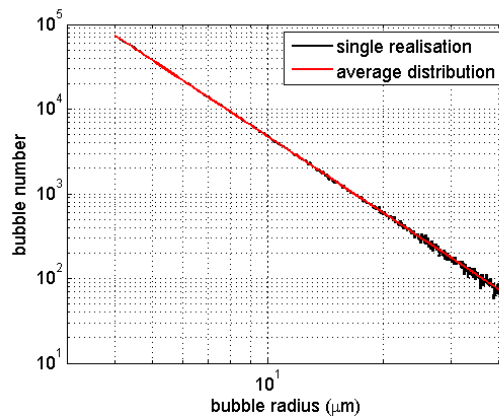


Figure 4. Bubble size distribution for single realisation (black curve) and averaged over 500 realisations (red curve).

The position of a bubble within insonified volume was generated randomly assuming a uniform distribution of bubbles within the beam element. In this simulation we used CW incident pulse modified by a Tukey window with parameter  $\alpha = 0.2$ . The amplitude of the pulse at the centre of the insonified volume can be calculated from the given source level of the transmitter,  $SL$ :

$$P_{ainc} = \varepsilon_s P_0 = 10^{-6} 10^{(SL/20)} / (2R_{tb}). \quad (26)$$

For  $R_{tb} = 10m$  and  $SL = 190dB$ , the incident pulse is shown in Figure 5.

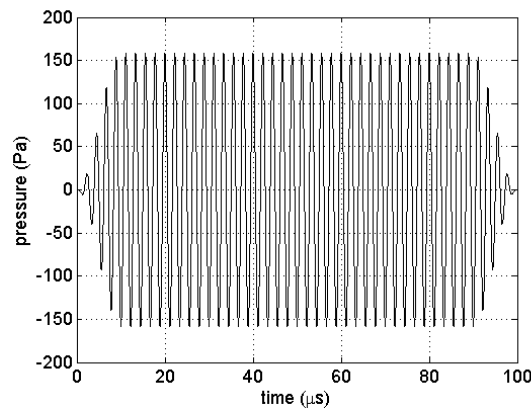


Figure 5. Incident pulse at the centre of insonified volume.

The total scattered pulse from the beam element is calculated according to equation (21). The scattered pulses from individual bubbles are pre-calculated for bubble radii at the centre of size bins at 1 m from bubbles. The pulse amplitude is then scaled by the distance from a specific individual bubble to the receiver,  $R_{rb}^{(k)}$ . The time of arrival of the scattered pulse at the receiver is calculated as  $t_k = (R_{tb}^{(k)} + R_{rb}^{(k)})/c_l$ . The pulses scattered from individual bubbles are summed coherently to form the total scattered pulse. An example of a scattered pulse from the beam element for a single realisation of bubble size and spatial distributions is shown in Figure 6.

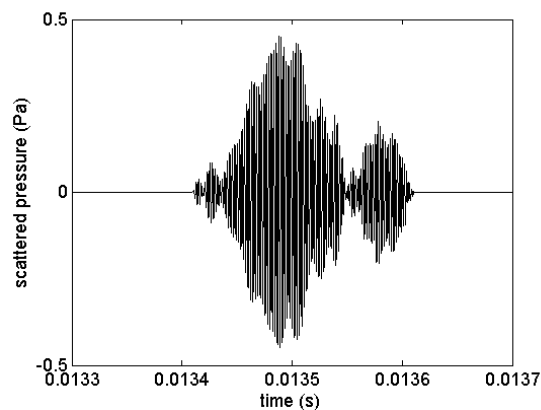


Figure 6. Scattered pulse as a summation of pulses scattered by individual bubbles in the insonified volume.

In simulation we can calculate the resulting scattered pulse from bubbles of a single size bin, and then compute the scattering cross-section by applying equations (18)-(20). The result of this for a single random realisation of bubble population in the insonified volume is presented as a black curve in Figure 7a. The red curve in this plot represents the scattering cross-section of a single bubble obtained from the numerical solution of the bubble oscillation equations. The results in the figure are presented in non-dimensional form. One can see significant fluctuations of the scattering cross-section for a single random realisation of the bubble population. Averaging results over many random realisations of the bubble population in the insonified volume smooths results as can be seen from Figure 7b, which shows results averaged over 500 random realisations. It is interesting to note that the scattering cross-section obtained from an ensemble of bubbles is slightly greater than that of a single

bubble of the same size in a small area near the resonant size of bubbles. This is because the solution for an ensemble of bubbles is based on the numerical solution for bubble oscillations, and the red curve in the plot represents the linear solution. Apparently, near resonance, the bubble oscillation is nonlinear, hence the difference in the scattering cross-section, similar to what we have seen in Figure 1 and Figure 2.

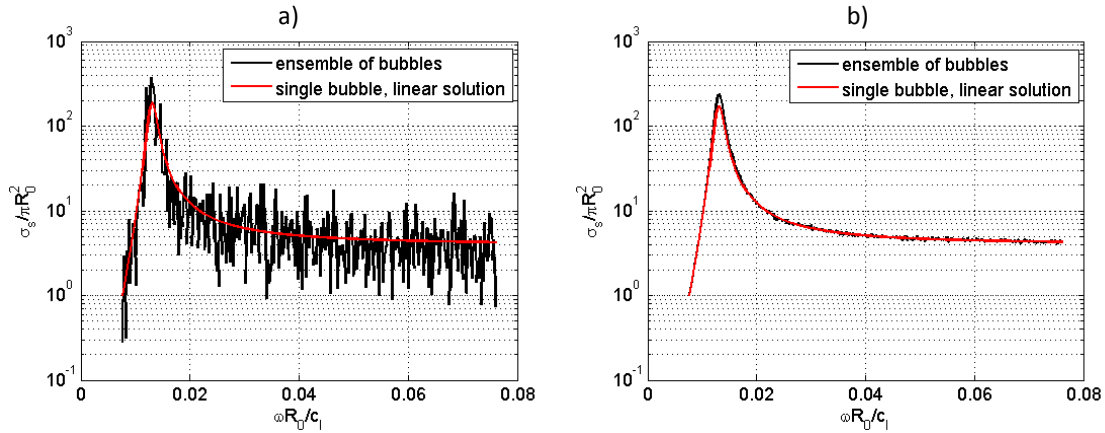


Figure 7. Scattering cross-section obtained from an ensemble of bubbles. a): single realisation of size and spatial distribution in the insonified volume. b): averaged over 500 realisations of bubble size and spatial distribution in the insonified volume.

By applying equations (18)-(20) to the total scattered pulse from the beam element, we can obtain the backscattering cross-section of the ensemble of bubbles per unit volume.

$$S_{bs} = 10^{(TS - \log_{10} V)/10}, \quad (27)$$

where  $TS$  is the target strength of the insonified beam element:

$$TS = -SL + RL + 20\log_{10} R_{tb} + 20\log_{10} R_{rb}, \quad (28)$$

and  $RL$  is the received signal level in dB:

$$RL = 20\log_{10} (|P_{rad}|/10^{-6}). \quad (29)$$

Figure 8 shows the results for 4500 random realisations of the bubble ensemble. One can see that the backscattering cross-section fluctuates significantly from realisation to realisation (black curve). The mean value (green curve) of the back-scattering cross-section per unit volume is higher than that based on the analytical linear solution for a single bubble (red curve):

$$S_{bs}^{\text{lin}} = \int_{R_{\text{min}}}^{R_{\text{max}}} n(R) \sigma_s^{\text{lin}}(R) dR, \quad (30)$$

where  $\sigma_s^{\text{lin}}$  is calculated from equation (14). It should be noted here that the red curve in Figure 8 shows not the mean value of the analytical backscattering cross-section but its value at a given random realisation of the bubble size distribution. One can see from the figure that it has only a very small variation. The magenta line in Figure 8 shows the backscattering cross-section per unit volume  $S_{bs}^{\text{num}}$  calculated via a similar method to equation (30) but based on the numerical solution for scattering cross-section of an individual bubble,  $\sigma_s^{\text{num}}$ . One can see that in this case, the mean value of the simulated backscattering cross-section per unit volume is very close to that based on the scattering cross-section of individual bubbles.

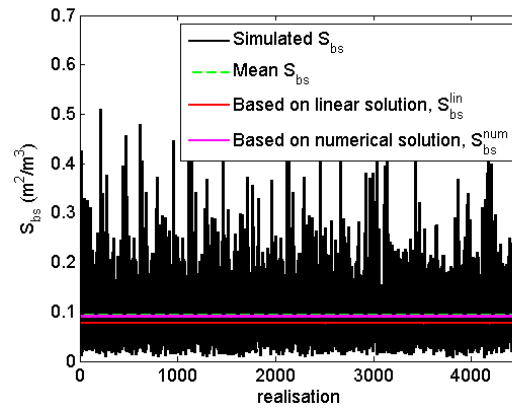


Figure 8. Variation of the backscattering cross-section per unit volume over 4500 realisations of bubble size and spatial distribution in the insonified volume.

Figure 9 shows the probability density function (pdf) of the simulated backscattering cross-section relative to its analytical value calculated from the given realisation of the bubble size distribution. The red curve in this figure shows that the simulated data can be fit well with the lognormal probability density function.

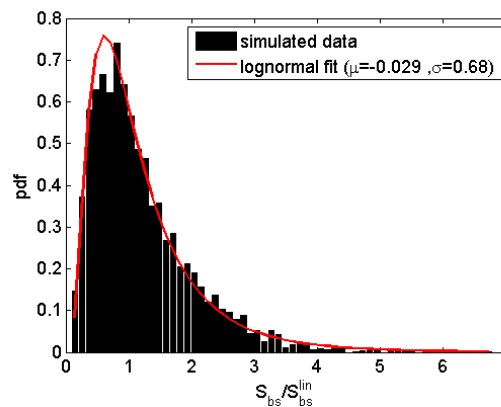


Figure 9. Probability density function of the relative backscattering cross-section per unit volume. Simulated data are based on 4500 bubble size and spatial distribution realisations. The red curve is a lognormal fit of the simulated pdf.

### 2.3 Representation of bubble cloud by point scatterers

Let us now consider a representation of the insonified bubble cloud volume (Figure 3) by a discrete number of point scatterers of uniform strength. The scattering strength of an individual point scatterer is calculated as follows:

$$\sigma_{s,ps} = \langle S_{bs} \rangle \frac{V}{N_{ps}}, \quad (31)$$

where  $\langle S_{bs} \rangle$  is the mean value of the simulated backscattering cross-section per unit volume calculated from a set of random realisations of the bubble size and spatial distribution in the insonified volume,  $N_{ps}$  is the number of point scatterers in the insonified volume,  $V$  is the insonified volume (equation 22). We consider the following number of the point scatterers: 3, 5, 10, and 100. For each number of the point scatterers we consider 4500 random realisations of their position within the insonified volume to simulate the backscattered pulse and the backscattering cross-section per unit volume of the insonified volume.

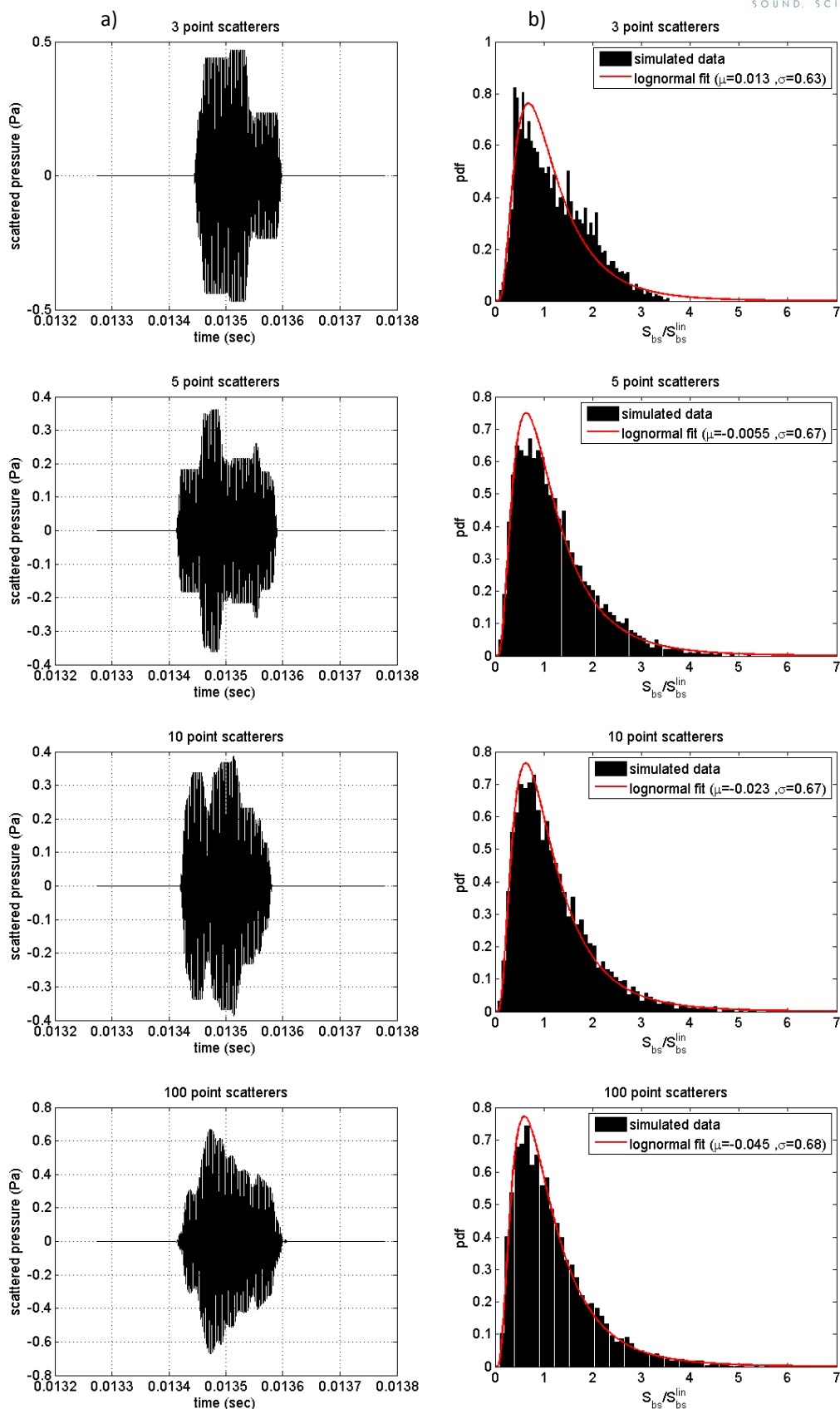


Figure 10. Representation of the insonified volume by point scatterers. a): example of a scattered pulse for one realisation of the point scatterers' positions. b): distribution of normalised values of the backscattering cross-section per unit volume for 4500 realisations of the point scatterers' positions. The number of point scatterers in one realisation, from top down: 3,5,10,100, as indicated also in the titles of the plots.

Figure 10 shows results of simulations for various numbers of point scatterers in the insonified volume. The left-hand side plots (Figure 10a) display an example of simulated backscattered pulses. Of course we should note here that the specific shape of the backscattered pulse changes significantly from realisation to realisation of the point scatterers' positions in the insonified volume. However, in the case of three or even five point scatterers one can clearly see that the backscattered pulse is a superposition of a corresponding number of individual scattered pulses, which are, for point scatterers, are scaled incident pulses. For ten and more point scatterers the scattered pulse has a more stochastic nature similar to the pulse simulated for the collection of large number of bubbles (Figure 6). Similar indications give the right-hand side plots (Figure 10b) showing the probability density function of the backscattering cross-section per unit volume relative to its analytical value based on a linear solution for individual bubbles (equation 30): for ten and more point scatterers the pdf is close to that obtained from a simulation using large number of bubbles (Figure 9).

### 3 CONCLUSIONS

A Monte Carlo model of acoustic scattering from a bubble cloud has been developed. Currently it is based on single scattering from individual bubbles, but a future model will take into account multiple scattering. The scattered pressure from individual bubbles is calculated from numerical solution of forced bubble oscillation in the acoustic field of incident pulse. The backscattered pulse from an insonified volume is calculated as a coherent summation of pulses scattered from individual bubbles. Simulations were performed for many realisations using realistic bubble size distributions, volume fractions, and sonar parameters. The simulations show, that the backscattered cross-section per unit volume of an ensemble of bubbles varies significantly with the realisation of the bubbles' positions in the insonified volume. The statistical distribution of the values of the backscattered cross-section per unit volume is well described by a log-normal probability density function for simulated parameters of sonar and bubble cloud.

Using the same model, representation of the insonified volume by a small number of point scatterers was tested. The scattering strength of the point scatterers was calculated from the mean value of the numerically simulated backscattering cross-section per unit volume of a bubble cloud. The results show that as few as ten point scatterers in the insonified volume are sufficient to produce a realistically looking backscattered pulse and reproduce sufficiently accurately the probability density function of the distribution of values of the backscattering cross-section per unit volume. The point scatterers' strength can be calculated from a known bubble size distribution and the scattering cross-section of individual bubbles, obtained either from a linear solution or from a numerical solution of bubble oscillation, if non-linear effects are estimated to be significant.

### REFERENCES

- Devin, Charles. 1959. "Survey of Thermal, Radiation, and Viscous Damping of Pulsating Air Bubbles in Water." *Journal of the Acoustical Society of America* no. 31 (12):1654.
- Eller, Anthony I. 1970. "Damping Constants of Pulsating Bubbles." *Journal of the Acoustical Society of America* no. 47 (5B):1469.
- Imagenex. *Imagenex model 881L digital multi-frequency imaging sonar. User guide* 2015. Available from <http://www.imagenex.com>.
- Keller, Joseph B., and Michael Miksis. 1980. "Bubble oscillations of large amplitude." *Journal of the Acoustical Society of America* no. 68 (2):628.
- Medwin, H, and CS Clay. 1998. *Fundamentals of acoustical oceanography*. Sydney: Academic Press.
- Prosperetti, A. 1977. "Thermal effects and damping mechanisms in the forced radial oscillations of gas bubbles in liquids." *Journal of the Acoustical Society of America* no. 61 (1):17-27.
- Wildt, R. 1946. "Acoustic Theory of Bubbles." In *Physics of Sound in the Sea*, 460-477.
- Yang, Xinmai, and C. C. Church. 2005. "A model for the dynamics of gas bubbles in soft tissue." *Journal of the Acoustical Society of America* no. 118 (6):3595-3606. doi: DOI: 10.1121/1.2118307.
- Zhang, Yuning. 2013. "A Generalized Equation for Scattering Cross Section of Spherical Gas Bubbles Oscillating in Liquids Under Acoustic Excitation." *Journal of Fluids Engineering* no. 135 (9):1.
- Zhang, Yuning, and Shengcai Li. 2014. "Thermal effects on nonlinear radial oscillations of gas bubbles in liquids under acoustic excitation." *International Communications in Heat and Mass Transfer* no. 53:43-49. doi: 10.1016/j.icheatmasstransfer.2014.02.005.
- Zhang, Yuning, and Shengcai Li. 2015. "Acoustical scattering cross section of gas bubbles under dual-frequency acoustic excitation." *Ultrasonics - Sonochemistry* no. 26:437-444. doi: 10.1016/j.ultsonch.2015.02.018.